ORIGINAL RESEARCH ARTICLE

Characterization and Corrosion Resistance of the Twin-Wire Arc Spray Al-5Mg Alloy Coating Applied on a Carbon Steel Substrate

Tuan Van Nguyen[1] · Thanh Duc Le[2] · Quy Thu Le[3] · Ha Thi Pham[1] ·
Anh Tuan Nguyen[1] · Ly Thi Pham[1] · Thuy Bich Dao[1] · Cuong Quoc Ly[1]

Abstract The Al-5Mg alloy coatings were fabricated by the twin-wire arc thermal spray on the SS400 steel substrate using various spraying parameters. The surface morphology of the coatings was examined using field emission scanning electron microscopy (FE-SEM). The porosity of the coatings was investigated by image analysis according to ASTM E2109-01 standard. The corrosion behavior of the coatings immersed in 3.5 wt.% NaCl solution was investigated by electrochemical polarization scanning and electrochemical impedance spectroscopy measurement. The study results showed that the coating deposited with a spray mode consisting of current of 300 A, pneumatic pressure of 5.5 bar, and standoff distance of 160 mm has higher Al and Mg elemental content than the coating fabricated with other spray parameters. The porosity of the coating varies from 7.38 to 11.82%, depending on the spray mode. The corrosion mitigation of the Al-Mg alloy coating was considerably enhanced due to higher contents of Al and Mg, a homogeneous surface, and low porosity.

Introduction

Carbon steel is one of the most commonly used materials in industries, accounting for roughly 85% of global steel products (Ref 1). Corrosion is the main cause of steel construction, especially in marine environments. Recent reports show that the cost of remedying the consequences of corrosion in seawater is up to 1.8 trillion USD per year (Ref 2). As a result, numerous scientists are always looking for anti-corrosion treatments in the maritime environment.

One of the most common and successful techniques for preventing corrosion is the application of coatings, especially metal coatings (Ref 3, 4). A variety of metal coatings, such as zinc coatings, aluminum coatings, aluminum alloy coatings, and zinc alloy coatings, have great application potential for anti-corrosion protection of structural steel in marine environments. These coatings protect the steel substrate via barrier and the sacrificial anode mechanisms (Ref 5, 6). Aluminum and zinc coatings offer high-quality anti-corrosion to steel substrates but have limitations. Zinc coatings have a short service life in marine environments, while aluminum coatings experience pitting corrosion in chloride-containing environments (Ref 7, 8). Several metal coatings such as zinc coatings, aluminum coatings, aluminum alloy coatings, and zinc alloy coatings have great application potential for corrosion protection of structural steel in marine environments, and aluminum alloy coatings are better than the rest (Ref 9, 10). Hot-dip galvanizing and thermal spraying are common technologies for metal coating (Ref 10-13), and thermal spray

✉ Thanh Duc Le
lethanha6@gmail.com

1 Institute for Tropical Technology, Vietnam Academy of Science and Technology, 18, Hoang Quoc Viet, CauGiay, Hanoi, Vietnam

2 Faculty of Mechanical Engineering, Le Quy Don Technical University, 236, Hoang Quoc Viet, CauGiay, Hanoi 100000, Vietnam

3 National Key Laboratory for Welding and Surface Treatment Technologies, NARIME, 4, Pham Van Dong, CauGiay, Hanoi, Vietnam

coating is recommended for metal coating applications to provide corrosion resistance to steel substrates in numerous environments (Ref 14-23. In recent years, flame spray and twin-wire arc spray have been used to fabricate metal coatings (Ref 24). The arc spray has many advantages, such as its flexibility and efficiency, low injection temperature, and low cost (Ref 25, 26). Studies on the corrosion resistance of metal coatings applied by arc spray and flame spray have received a lot of attention from researchers.

Kuroda et al. (Ref 27) studied the corrosion resistance of zinc, aluminum, and ZnAl alloy coatings after an 18-year test at the seaside in Chiba, Japan. The test results show that most of those coatings retain good corrosion resistance, in addition to the Zn coatings. The Zn-13Al and Zn-15Al alloy coatings are created by twin-wire arc spray and flame spray. The research results show that the Zn-Al alloy coatings have much higher corrosion resistance than the pure zinc and aluminum coatings (Ref 9, 28). The influence of sulfate-reducing bacteria (SRB) in seawater on the corrosive behavior of zinc, aluminum, and Zn-15Al alloy coatings fabricated by arc spray was studied by L. Qiao et al. (Ref 29). The findings of the experiment indicate that Al_2O_3 corrosion products formed of the surface of the aluminum and Zn-15Al coatings created biofilms that contribute to improving the corrosion protection ability of coatings in marine environments. In addition, the corrosion protection of Zn-15Al coating fabricated by twin-wire arc spray in seawater containing SRB was studied by S. Hong et al. (Ref 30). The obtained results demonstrate that the silicone resin-sealed Zn-15Al coating has a charge transfer resistance that is ten times greater than that of the non-sealing treatment. However, the amount of elemental sulfur present in the untreated coating is less than half of that in the seal-treated coating. The coating's corrosion rates increased after the first time of exposure to seawater containing SRB and decreased during an 8-day test period. In 2013, Katayama et al. (Ref 31) conducted a study about the corrosive properties of Al, Zn, and Zn-30Al coatings created by flame spray. Coatings are naturally tested in marine environments for 33 years. The research results show that the corrosion products consisting on the surface of the Zn-30Al coating have contributed to better corrosion protection compared to the pure Zn, Al coatings. Along with the deposit of Zn, Al, and Zn-Al alloy coatings by thermal spraying, pseudo-alloy coatings have also been researched in recent years. In 2019, Lee et al (Ref 32) invested in a study on the corrosion kinetics and mechanism of Zn-Al pseudo-alloy coating with 28 wt.% Al and 68 wt.% Zn in the 3.5 wt.% NaCl solution. The coating was deposited by the twin-wire arc spray. According to study findings, the coating's ability to prevent corrosion over a 55-day immersion period was improved by the corrosion product

$Zn_5(OH)_8Cl_2.H_2O$ that is present on its surface. The anti-corrosion of Zn-15Al, Zn-30Al, and Zn-50Al pseudo-alloy coating in NaCl solution has been studied by Hu et al. (Ref 33), and the coating was deposited by arc spray. Research results show that the corrosion rate of Zn-30Al coating is the lowest of the three coatings. In 2022, Yasoda and colleagues from North Dakota State University, Fargo, USA (Ref 34), surveyed the corrosion properties of Zn-15% pseudo-alloy coating and Zn-15Al alloy coating in the containing environment chloride. The research results show that the Zn-15% pseudo-alloy coatings have anti-corrosion resistance better than the Zn-15Al alloy coating, about four times. The corrosion resistance of the pseudo-alloy coating is greater than that of the alloy coating because the pseudo-alloy coating contains more aluminum than the alloy coating (Ref 34).

Regarding the Al-Mg alloy coating, the research results of I. Park et al. show that the Al-Mg alloy deposited by the electric arc spraying process has better resistance to aggressive corrosion compared with pure aluminum coatings (Ref 35). In 2014, a group of Korean scientists Choe (Ref 17) conducted research on the corrosion protection ability of Al, Zn-27Al, and Al-5Mg coatings. Investigation results showed that Al-5Mg alloy coating had a higher corrosion protection ability than the rest. In addition, the ability of the Al-5Mg coating to protect the steel substrate in salt spray tests for a total time of 14,000 h has been confirmed by Takeyoshi et al. (Ref 23). According to our research, the corrosion behavior of the Al-5Mg alloy coating fabricated by the twin-wire arc spray process has not been published much in the world. In this study, we focused on studying the affectation of the arc spray modes on the corrosion properties of the Al-5Mg alloy coating. In this work, the corrosion behavior of Al-5Mg alloy coating is immersed in a solution of 3.5 wt.% NaCl for 6, 24, 48, 96, and 240 h was investigated.

Experimental

Materials

SS400 steel plate in the size of $50 \times 50 \times 3$ mm (C: 0.15%; Si: 0.14%; Mn: 0.45%; Ni: 0.03%; Cr: 0.02%; P: 0.02%; S: 0.03%) was supplied by Suzuki Vietnam Special Steel Co., Ltd. Al-Mg alloy wire with 2 mm in diameter (Mn: 0.3%; Mg: 5.0%) was supplied by Metallisation Co., Ltd (UK).

Coating Preparation

The SS400 steel surfaces were cleaned with acetone and roughened with 1-1.2 mm brown corundum abrasive provided by Vietnam Hai Duong Joint stock Grinding

Table 1 The spray parameters

No.	Parameters	AM1	AM2	AM3
1	Arc voltage, V	32		
2	Spray current, A	150	200	300
3	Air pressure, bar	4	4.5	5.5
4	Spray distance, mm	100	200	160
5	Spray angle	90°		

Company before creating the Al-Mg alloy coating. The coatings were deposited by the twin-wire arc spraying process, using a device OSU Hessler 300A (Germany) with the parameters shown in Table 1. The Al-Mg alloy coatings have a thickness of about 300 μm. There are three coating types of samples denoted as AM1, AM2, and AM3.

Coating Characterization

The cross-sectional structure and the surface morphology of the coatings were determined by field emission scanning electron microscopy (FE-SEM) using Nova Nano SEM (Japan) and optical microscope GX53 Olympus (Japan), respectively. The thickness and porosity of the coatings were analyzed according to ISO 1463:2003 (Ref 36) and ASTM E2109-01 (Ref 37).

The x-ray diffraction analysis (XRD) utilizing instrument EQUINOX 5000, Fr instruments was used to ascertain the phase compositions of the coatings, with 2θ angle scanned, from 0.1° to 120°, scanning step of 0.0154°/s, wavelength $\lambda = 1.54056$ Å. The elemental compositions on the surface of coatings were determined by energy-dispersive x-ray spectroscopy (EDX) using instrument SEM JSM-6510LV.

Electrochemical Corrosion Tests

In testing practice, a polarization cell is setup consisting of an electrolyte solution of 3.5 wt.% NaCl, a reference electrode of Calomel electrode SCE Hg/Hg2Cl2 (saturated KCl), a counter electrode of platinum metal with an area of 1cm2, and the working electrode of 1 cm^2 area Al-Mg alloy coating. The electrodes are connected to a Biologic VSP-300 electronic instrument (France). The 1 cm^2 area Al-Mg alloy coating is the working electrode. The electrochemical corrosion behavior of the coating was analyzed by potentiodynamic polarization according to ASTM G59 (Ref 38) and measuring the EIS over time after 6, 24, 48, 96, and 240 h. The polarization curves were obtained at a scan rate of 0.1667 mV/s from −30 to 30 mV/SCE around the open circuit potential (Eocp). Impedance values were recorded in the frequency range performed from 104 to 10-2 Hz, 10

points/decade with a sinusoidal oscillation with amplitude ±10 mV (Ref 39).

Results and Discussion

Coating Characterization

Surface Morphology and Composition of the Coating

The twin-wire arc spray process has the electric arc, which generates high temperature (>40,000 °C), causing the Al-Mg alloy in wire form to almost completely melt. The molten Al-Mg alloy is then atomized and projected towards the substrate at a high speed (>200 m/s) by the compressed air flow forming a coating (Ref 40). The resulting coating has a rather complex structure including pores, cracks of non-melting, semi-molten, fully melted and splats, etc. The structure of Al-Mg alloy coating is influenced by the twin-wire arc spray parameters. The surface morphology of Al-Mg alloy coating deposited by the twin-wire arc spray process with various parameters (Table 1) is shown in Fig. 1. Research results show that the surface of the AM3 sample has the most homogeneous structure compared to the AM1 and AM2 samples. The sample AM3 has almost no non-molten metal particles that exist on the surface. Meanwhile, the sample AM2 appeared to have more non-molten metal particles than the AM1 and AM3 samples. The AM2 sample was sprayed with a higher spray current than the AM1 sample, so the Al-Mg alloy is supplied with a higher energy source, and the injection material melted more than the AM1 sample. However, the AM2 sample has an injection distance longer than the AM1 sample, which results in the molten metal particles during the spraying process of the AM2 sample being more oxidized by exposure to the air, causing the surface of the AM2 sample to be oxidized, lead to its structure less homogeneous than samples AM1. Sample AM3 was sprayed with a higher spray current than that of the AM1 and AM2 samples, so semi-molten metal particles presented in the AM3 sample are less than that of the AM1 and AM2 samples, so the coating surface of the AM3 sample had a structure more homogeneous than the AM1 and AM2 samples.

Figure 2 is the result of SEM-EDS analysis to determine the composition of chemical elements present in the Al-Mg alloy coating. Analysis results (Table 2) show that there is an O element in the Al-Mg alloy coating in addition to Al and Mg elements, the O element in the coating is due to the process of spraying and manufacturing the material, a part of the Al-Mg particles has been oxidized due to high temperature. The mass composition of element O in the AM2 sample is the highest of the three samples, while the elemental composition of Al and Mg of the AM2 sample is

Fig. 1 SEM images of Al-Mg alloy coatings
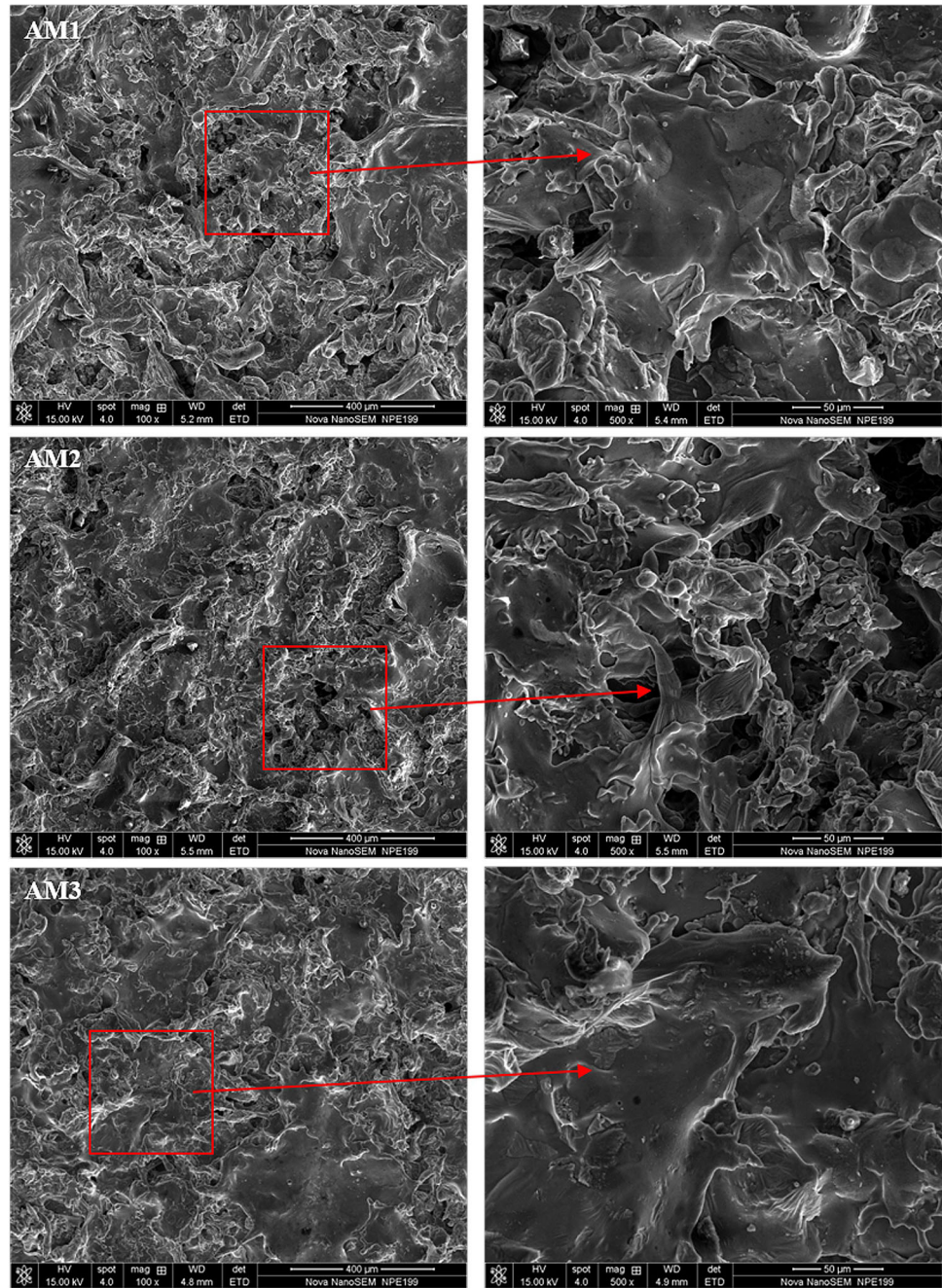
the lowest. It shows that the coating was sprayed with a longer spray distance, and the molten Al-Mg material oxidized and evaporated after it was out of the spray gun head due to the contact time of the spray material with atmospheric oxygen. In addition, during the coating process, due to being melted at high temperatures, the metals are vaporized, making elements Al and Mg content in the coating lower than that of the material. The content of Al and Mg has different changes depending on the spray parameters. Research results show that the ratio of element Mg/Al in AM3 coating is the highest in the three coating samples. It shows that the Al-5%Mg alloy coating is sprayed with a spray current of 300 A, pneumatic pressure of 5.5 bar, standoff distance of 160 mm, which limits the amount of elements Al and Mg consumed in the spray process.

**Fig. 2** SEM-EDS analysis images of Al-Mg alloy coatings
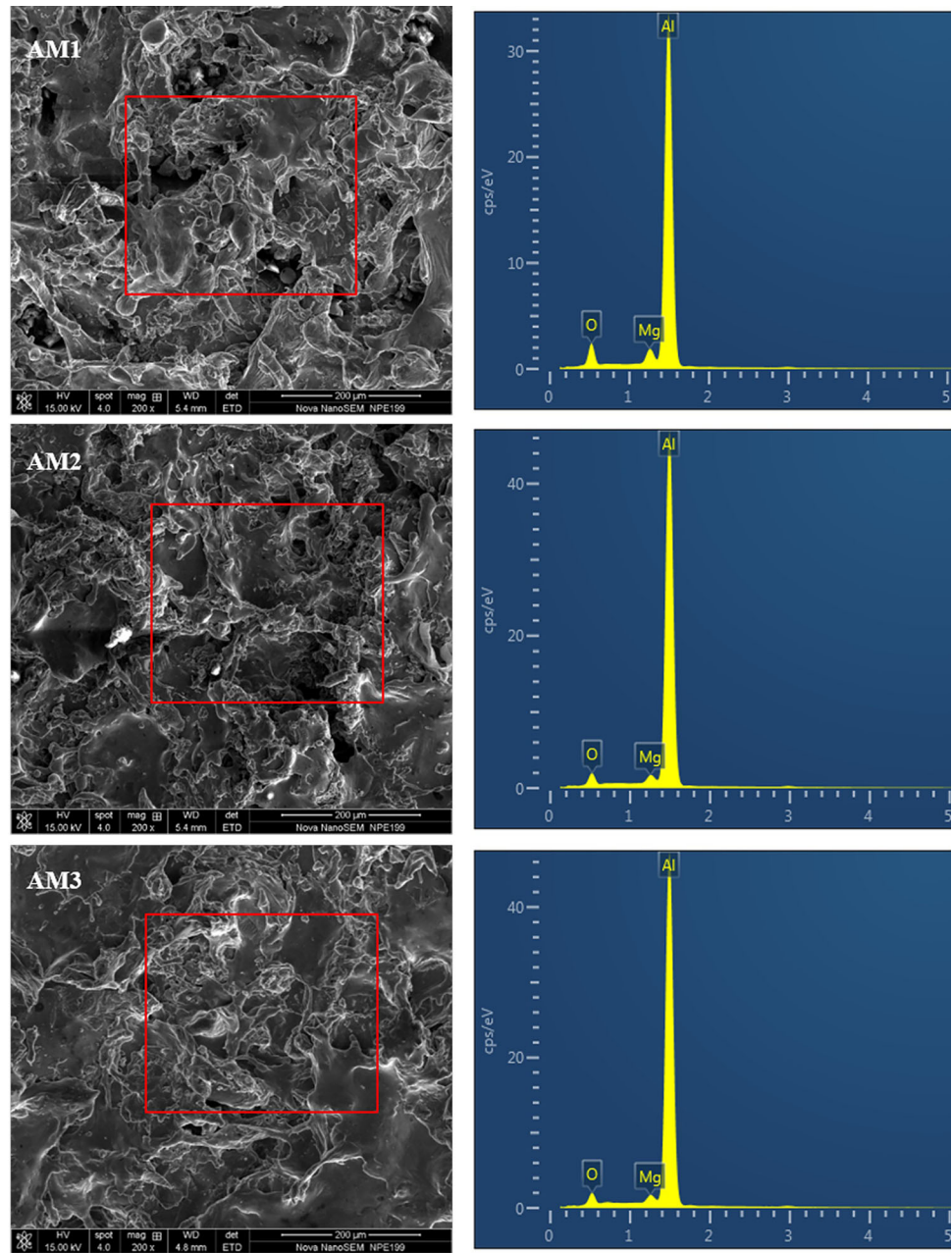
Table 2 Chemical elemental composition of coatings

No.	Element	Mass composition, %		
		AM1	AM2	AM3
1	Al	84.17	77.13	85.78
2	Mg	2.84	2.46	3.47
3	O	12.99	20.42	10.75
	Total	100	100	100

Cross-Sectional Structure and Porosity of the Coating

The Al-Mg alloy coating deposited by the twin-wire arc spray process has a characteristic structure of thermal spray coatings, including sheet structure, small cracks, very small infight particles (nano-size), oxides, semi-molten particles, and pores (Ref 32, 41). Figure 3 shows the Al-Mg alloy coating microstructure fabricated by the twin-wire arc spray method. There are two types of oxides that can exist in the coating, one that is formed separately, and the other
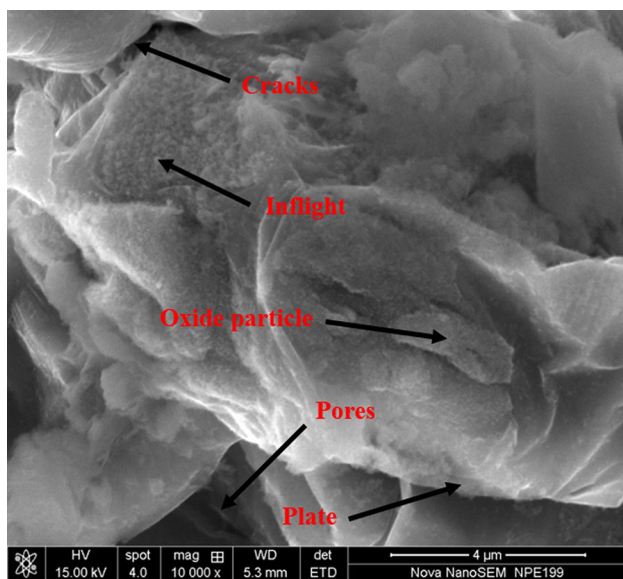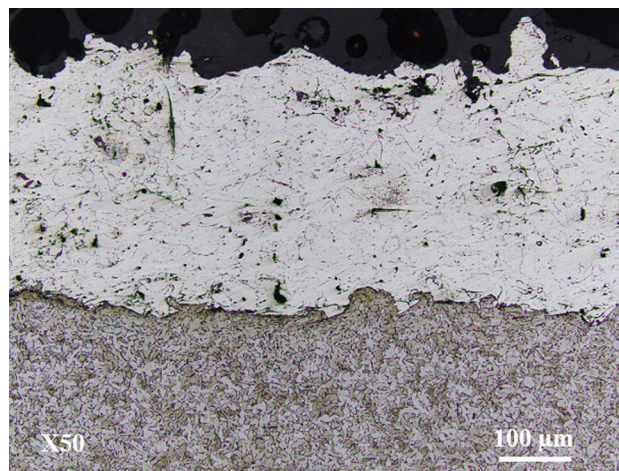
Fig. 3 Microstructure of Al-Mg (AM3) alloy coating

Fig. 4 The cross-sectional structure of Al-Mg (AM3) alloy coatings

that is wrapped around the deformed metal elements. The first type is generally considered to be detrimental, worsening the coating's mechanical properties. The latter has the role of bonding separate metal elements. The cross-sectional image of the Al-Mg alloy coating shown in Fig. 4 shows that the coating has a thickness of about 300 μm including metals with a sheet structure. Sheets of metal with different shapes are separated by a thin oxide layer with a thickness of about 1 μm. In addition, in the Al-Mg alloy coating, there are pores, cracks, and defects with different shapes that are not tightly connected. The loose association of metal elements when deformed gives the coating a characteristic porosity.

The porosity of the Al-Mg alloy coating was analyzed by image analysis software on cross-sectional structures (Fig. 5) according to ASTM E2109-01 (Ref 37). Analyzes were performed at 5 different locations on the cross-section of the polished coating with a length of about 25 mm (Ref 37). The measured porosity values are the average of the analyzed sites. The analysis results showed that the samples AM1 and AM2 had porosity of about 10.87 and 11.82%, respectively. Meanwhile, the sample AM3 had a porosity of about 7.38%, which is significantly lower than that of the AM1 and AM2 samples. The sample AM3 was sprayed with a spray pressure (5.5 bar) higher than that of the AM1 and AM2 samples. Particles sprayed to the surface with high air pressure have high kinetic energy leading to the low porosity of the coating (Ref 42-44). On the other hand, the AM3 sample was sprayed with a high spray current, which makes the metal particles completely melt, depositing a coating with high density. Therefore, the AM3 coating sample had the lowest porosity of the three types of samples.

Phase Composition

The results of studying the phase composition of Al-Mg wire materials and coatings are illustrated in Fig. 6.

The results show that Al-Mg wire has Al (cubic) and Al_2MgO_4 (cubic) crystals as the main phase. The Al-Mg alloys with a high aluminum content (>3%) will form a supersaturated solid solution with a phase composition of Mg_5Al_8 (Ref 45). However, on the XRD diagram of Fig. 6, no characteristic peaks of the Mg_5Al_8 crystalline phase were observed in AlMg wire. The Mg_5Al_8 crystalline phase composition was not found in Al-Mg wire, possibly due to the small content of Mg_5Al_8 or the amorphous form of Mg_5Al_8. For the coating samples (AM1, AM2, AM3), in addition to the Al (cubic) and Al_2MgO_4 (cubic) crystalline phases found in the coating, there is also an Al_3Mg_2 (cubic) phase composition appearing at an angle of 2θ around 35° and 38°. This shows that there was a phase change during the coating spraying process due to the impact of high-temperature Al and Mg interacting to form the Al_3Mg_2 intermetallic phase. The presence of the Al_3Mg_2 phase contributes to an increase in the hardness of the Al-Mg coating and reduces the corrosion resistance of the coating (Ref 46, 47).

Corrosion Behavior of the Coatings

Potentiodynamic Polarization

The electrochemical corrosion behavior of SS400 steel substrate after 1 h immersed in 3.5 wt.% NaCl solution is shown in Fig. 7(a). The polarization curve of the SS400 steel substrate was scanned around the open circuit potential (OCP) in the range of −500 to 500 mV, scanning speed of 0.2 mV s^{-1} (Ref 48). Corrosion current density and

Fig. 5 The porosity of Al-Mg alloy coating samples
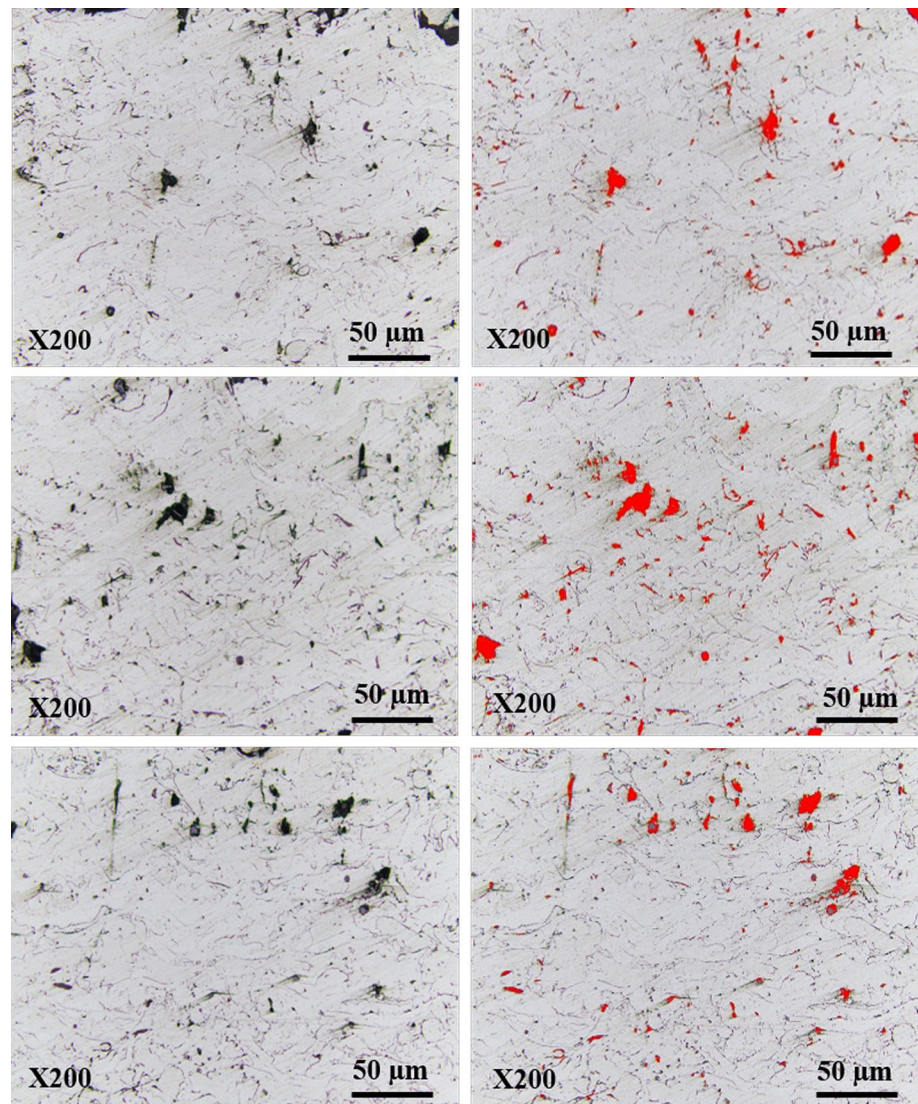
corrosion potential of SS400 steel substrate are 0.548 µA/cm^2 and −515.20 mV/SCE, respectively, determined from EC-Lab software. Meanwhile, the electrochemical corrosion parameters of the coatings in the solution of 3.5 wt.% NaCl over time were determined by the dynamic potential polarization method according to ASTM G59 (Ref 38). Dynamic potential polarization curves of coatings in NaCl solution over time are shown in Fig. 7(b-d). The electrochemical data obtained from the polarization curves of the samples over time are illustrated in Table 3.

Research results show that, after 6 h of exposure, the corrosion current density of sample AM2 (27.1 µA/cm^2) is much higher than that of the samples AM1 (3.3 µA/cm^2) and AM3 (2.7 µA/cm^2). It shows that the surface morphology as well as the porosity and aluminum element composition in the coating significantly affect the corrosion rate of the Al-Mg coating. The AM2 coating has a lower

aluminum content than the AM1 and AM3 samples, so the AM2 has a higher corrosion rate than the AM1 and AM3 samples (Ref 34). Sample AM3 has lower porosity than the samples AM1 and AM2, so the corrosion rate of the sample AM3 in NaCl solution has a lower value than that of the AM1 and AM2 samples. Compared with the SS400 steel substrate, the coating samples had a lower corrosion potential in the NaCl solution at all time points of the investigation. It shows that, in the NaCl solution, the Al-Mg coating protects the substrate according to the sacrificial anode mechanism. The samples' corrosion current density in the NaCl solution varied differently over time.

The sample AM1 had an increased corrosion current density from 3.3 to 13.2 µA/cm^2 when it was immersed in NaCl solution for a period of 6-24 h. It shows that the inside of the coating of sample AM1 had a complex structure with many cracks and pores, which promoted the

Fig. 6 X-ray diffraction pattern
to determine phase composition
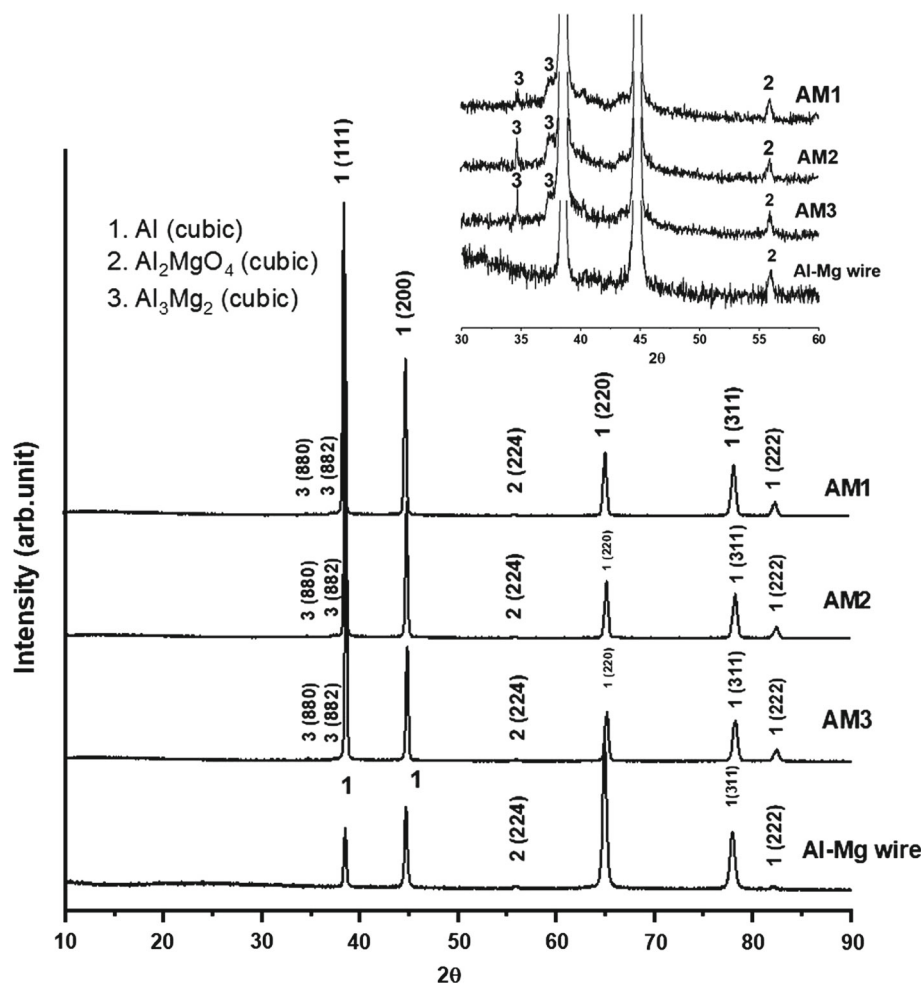
corrosion process of the coating from 6 to 24 h. After 24-240 h of exposure, the corrosion current density of sample AM1 did not change significantly, in the range from 12 to 13 µA/cm².

For the sample AM2, the corrosion current density tended to decrease from 27.1 to 11.5 µA/cm² during the immersion period of 6-48 h. The coating of the AM2 sample had an inhomogeneous surface structure with high porosity and corrosion rate. Corrosion products have accumulated in the coating causing the porosity and corrosion rate of the coating to decrease (Ref 31). However, after immersion time from 48 to 240 h, the corrosion current density tends to increase sharply. It can be explained that some part of the corrosion products has been separated, causing the coating porosity to increase, leading to an increase in the corrosion rate of the coating. In addition, the investigation results show that the value of the corrosion potential of the AM2 sample tends to increase gradually over time. It shows that the corrosion process under the influence of the steel substrate was increased over time because the NaCl solution penetrated the coating to the steel substrate through the pores.

Regarding the sample AM3, the research results showed that, after immersion time from 6 to 24 h, the corrosion current density increased by approximately 42% from 2.7 to 3.9 µA/cm². It shows that the corrosion process in NaCl solution took place on the surface and inside the coating. After immersion time from 24 to 48 h, the corrosion product had not enough time to diffuse out and accumulate in the coating, making the corrosion density of the AM3 sample decrease by about 84% from 3.9 to 2.1 µA/cm². However, after exposure time from 48 to 240 h, the corrosion current density has been trending upward. It can be seen that the corrosion products contained in the coating have been diffused out, increasing the porosity of the coating, and leading to an increase in the corrosion rate of the coating. During the immersion time from 24 to 96 h, the corrosion potential of the AM3 sample steadied at a potential of about 1000 mV/SCE, then the corrosion potential tended to increase close to the steel substrate's corrosion potential. It shows that the NaCl solution may have penetrated through the AM3 coating to the substrate after 96 h of immersion.
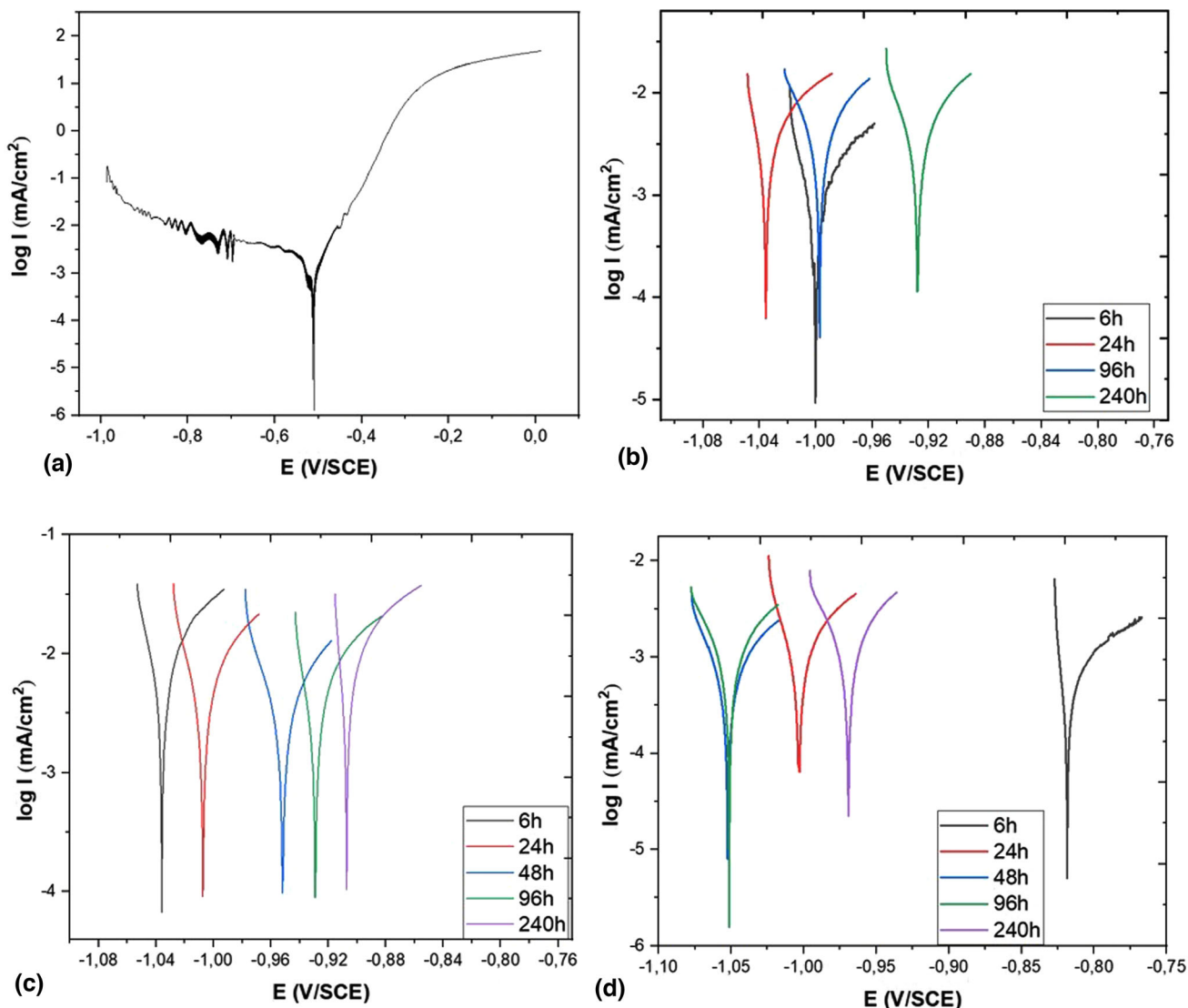
Fig. 7 Polarization curves of SS400 steel base (a) and coating samples AM1 (b), AM2 (c), AM3 (d) in 3.5 wt.% NaCl solution

Electrochemical Impedance Spectroscopy (EIS)

The EIS technique impressively investigates and differentiates different electrochemical processes in the coating over a wide frequency range (Ref 34). The results of measuring the total electrochemical resistance of the coating samples in a solution of 3.5 wt.% NaCl over time are shown in Fig. 8. Thermal spray coatings are heterogeneous, so the constant phase element CPE (Q) is used as a substitute for the ideal capacitance in the electrical equivalent circuit (EEC) (Ref 49). In addition, the coating corrosion process involves a diffusion element (W) due to corrosion products. Q/CPE and W depend on the frequency according to the following equation (Ref 50):

$$Z(f) = \frac{1}{Q(i2\pi f)^n}$$

$$Z(f) = \frac{\sqrt{2}}{\sqrt{2\pi f}} n$$

Z: Impedance; Q/CPE: the constant phase element; i: the imaginary number; f: the frequency in Hz; n: phase angle between imaginary axis ($-$Im $(Z)>0$) and real axis Re(Z)

Therefore, the electrical equivalent circuit $R1\, Q1/(R2\, Q2/(R3\, W3))$ (Fig. 9) was chosen to describe the electrochemical processes occurring in the coating for the exposure periods (Ref 39), where $R1$ is the resistance of the solution between the working electrode and the reference electrode, $R2$ is the resistance of the pore, and $R3$ is the polarization resistance of the surface. $Q1$ is related to the

Table 3 Electrochemical parameters obtained from extrapolation of Tafel at various times of exposure in the solution of 3.5 wt.% NaCl

No.	Sample ID	Immersion time	i_{corr}, µA/cm²	E_{corr}, mV/SCE	R_p, Ω cm²
1	AM1	After 6 h	3.3	−1002.26	7.994×10^3
		After 24 h	13.2	−1034.57	1.979×10^3
		After 48 h			
		After 96 h	12.1	−997.16	2.159×10^3
		After 240 h	12.4	−927.50	2.098×10^3
2	AM2	After 6 h	27.1	−1035.55	0.962×10^3
		After 24 h	18.0	−1007.01	1.448×10^3
		After 48 h	11.5	−951.45	2.266×10^3
		After 96 h	16.2	−928.45	1.606×10^3
		After 240 h	26.7	−907.07	0.975×10^3
3	AM3	After 6 h	2.7	−817.97	9.573×10^3
		After 24 h	3.9	−1049.82	6.726×10^3
		After 48 h	2.1	−1052.05	12.385×10^3
		After 96 h	3.1	−1051.10	8.303×10^3
		After 240 h	4.0	−969.29	6.521×10^3

double layer of the solution/coating. $Q2$ is related to the double-layer capacitance of the solution/inner surface. $W3$ is related to diffusion due to the formation of corrosion products. The corrosion product of Al-Mg alloy coating in solution is formed according to the following reactions (Ref 51).
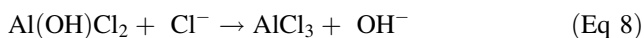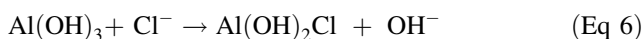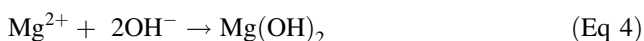
Al and Mg always preferentially dissolved owing to their anodic nature at the anodic location to form Al^2 and Mg^2 in their coatings, respectively:

$$Mg \rightarrow Mg^{2+} + 2e^- \qquad (Eq\ 1)$$

$$Al \rightarrow Al^{3+} + 3e^- \qquad (Eq\ 2)$$
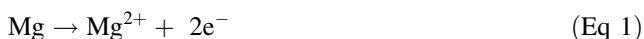
The oxygen reduction reacts at the cathodic:

$$O_2 + 2H_2O + 4e^- \rightarrow 4OH^- \qquad (Eq\ 3)$$

The corrosion products:

$$Mg^{2+} + 2OH^- \rightarrow Mg(OH)_2 \qquad (Eq\ 4)$$

$$Al^{3+} + 3OH^- \rightarrow Al(OH)_3 \qquad (Eq\ 5)$$

$$Al(OH)_3 + Cl^- \rightarrow Al(OH)_2Cl + OH^- \qquad (Eq\ 6)$$

$$Al(OH)_2Cl + Cl^- \rightarrow Al(OH)Cl_2 + OH^- \qquad (Eq\ 7)$$

$$Al(OH)Cl_2 + Cl^- \rightarrow AlCl_3 + OH^- \qquad (Eq\ 8)$$

In the Nyquist diagram (Fig. 8), the solid curves represent the simulated calculated data from the EEC diagram, using EC-Lab software (Bio-Logic). The error between calculated data and experimental data is evaluated based on the values of χ^2. Accordingly, the data obtained in Table 4 from the EEC with χ^2 have the smallest value after some fitting processes (Ref 39, 48). The factors were calculated to have an error of less than 10%.

The measurement results of the EIS of the AM1 sample after 6 h of immersion in the solution show that (Fig. 8), there are two half-semicircular loops on the Nyquist diagram and two inflection points on the Bode plot. The first half-semicircular loop at mid-frequency is related to the corrosion process of the coating (Ref 52). The second half-semicircular loop is related to corrosion products that were deposited on the surface (Ref 53). The first and second half-semicircular loops are gradually smaller during the immersion time from 6 to 48 h related to the corrosion process inside the coating due to the NaCl solution penetrating the coating through the pores. During the sample exposure period from 48 to 240 h, the measurement results of the EIS tend to increase gradually. This is explained by the corrosion products of the coating in the NaCl solution that were formed over time which covered the surface of the coating and blocked the pores and defects. After 96 h of immersion, the phase angle maxima shown on the Bode plot in the average frequency range shifted toward the lower frequency direction. The phase angle at high frequencies approaches the value of 0°. It shows that the corrosion products have high impedance and high insulating ability (Ref 53-55). The increase in the double layer capacitance (Q) value of the AM1 sample, together with the increase in Z-modulus and phase angle at mid-low frequencies, caused the bias resistance of the coating to tend to increase during the sample immersion time from 48 to 240 h due to a change in the corrosion properties of the surface during the above exposure time (Ref 56). During the sample immersion period from 48 to 240 h, the corrosion products deposited in the pores of the coating gradually increased, causing the pore resistance of the coating to increase. The analytical results in Table 4 show that the $R2$ of the AM1 sample immersed in NaCl solution increased from 164 to 1430 Ω cm² after immersion time from 48 to 240 h. On the other hand, the analysis results
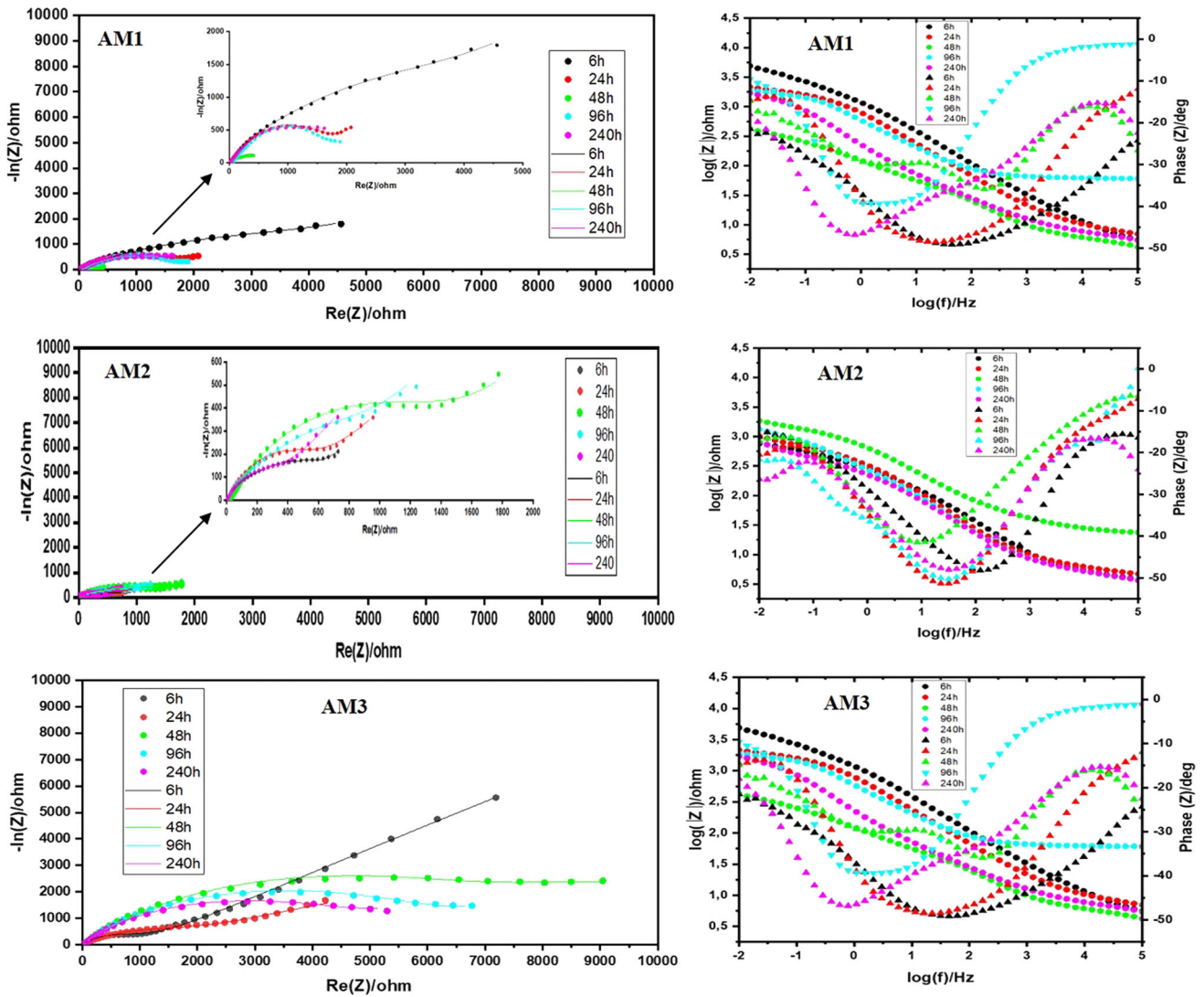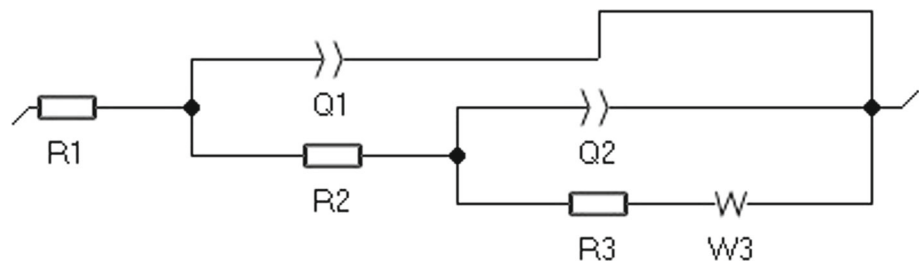
Fig. 8 Impedance spectra of the samples AM1, AM2, and AM3 immersed in 3.5 wt.% NaCl solution at various times

Fig. 9 The electrical equivalent circuit used to fit the EIS data of samples AM1, AM2, and AM3

show that the $R3$ of sample AM1 had different values over time, which shows that the formed corrosion products accumulated and separated from the surface of the coating sample leading to the surface coating changing differently over time.

The EIS of the AM2 sample shown in Fig. 8b shows that there are two half-semicircular loops on the Nyquist diagram and two inflection points on the Bode plot similar to sample AM1 at all times of sample measurement. The half-semicircular loop at high frequencies is related to the

**Table 4** Simulative electrochemical parameters obtained from Nyquist plots at various immersion times

Samples ID	Immersion time, h	R_1, Ω cm^2	Q_1, Fcm^{-2} s^{-n}	n_1	R_2, Ω cm^2	Q_2, Fcm^{-2} s^{-n}	n_2	R_3, Ω cm^2	s_3, Ωs$^{-0.5}$
AM1	6	3.706	0.244×10^{-3}	0.559	4266	1.82×10^{-3}	0.996	1266	262.8
	24	6.68	0.335×10^{-3}	0.590	1538	0.116×10^{-3}	0.467	554	112.1
	48	3.578	1.852×10^{-3}	0.581	164	$1.85 \times 10^{-}$	0.747	241	21.52
	96	3.60	0.347×10^{-3}	0.661	893.5	0.234×10^{-3}	0.994	878.8	40.96
	240	3.633	1.502×10^{-3}	0.740	1430	$4.93 \times 10^{-}$	0.750	356	20.42
AM2	6	3.635	0.548×10^{-3}	0.612	400.5	$2.427 \times 10^{-}$	0.738	281	40.9
	24	5.001	0.683×10^{-3}	0.513	778	11.6×10^{-3}	0.750	329	73.43
	48	18.82	$0.393 \times 10^{-}$	0.637	1258	5.829×10^{-3}	0.769	435.3	109.1
	96	3.976	0.875×10^{-3}	0.609	803	1.844×10^{-3}	0.75	554.4	74.37
	240	3.656	1.128×10^{-3}	0.573	600	19.09×10^{-3}	0.85	415.4	52.2
AM3	6	7.521	0.016×10^{-3}	0.737	1007	0.318×10^{-3}	0.724	5584	2903
	24	8.135	51.95×10^{-3}	0.610	1089	0.256×10^{-3}	0.625	2715	491.1
	48	10.34	0.102×10^{-3}	0.644	8936	4.253×10^{-3}	0.932	2743	133.8
	96	4.278	0.124×10^{-3}	0.600	6334	5.140×10^{-3}	0.771	340	239.4
	240	9.533	0.216×10^{-3}	0.705	5017	6.810×10^{-3}	0.703	179.7	190.5

electrochemical process of the solution/coating. The second half-semicircular loop is related to the electrochemical process of the solution/inner surface of the coating (Ref 57). The Bode plot in Fig. 8b illustrates the phase angle at the high frequency of sample AM2 tends to gradually increase to 0° during the period of sample immersion from 6 to 96 h. It shows that the corrosion product of the AM2 sample generated on the coating surface increases over time. Corrosion products formed as the polarization resistance of the R_p surface tended to increase over time from 281 to 554 Ω cm^2 (Table 4). Phase angle values in the mean frequency range after 48 h of immersion are higher than those of immersion at other times. The analysis results show that the pore resistance $R2$ of the AM2 sample after 48 h of immersion is 1258 Ω cm^2, which is higher than that of other values. It shows that the corrosion products of sample AM2 formed and accumulated in the holes of sample AM2 after 48 h of immersion, limiting the corrosion rate of the coating, making the measured corrosion current density of the AM2 sample 11.5 μA/cm^2, significantly lower than that of AM2 sample soaked in NaCl solution after 6, 24, 96, and 240 h. $R2$ of sample AM2 tends to decrease gradually after 48 h of immersion. This is explained by the high porosity of the AM2 sample, which allows the NaCl solution to penetrate much in the coating, increasing the corrosion rate of the AM2 sample gradually after 48 h of immersion. Meanwhile, $R3$ of sample AM2 fluctuated over time after 24 h of immersion. That shows the surface of the AM2 sample has different changes in the sample immersion time after 24 h because the AM2 sample

has a more complex surface structure than the AM1 sample.

For sample AM3, the results of EIS analysis (Fig. 8c) show that there are two half-semicircular loops on the Nyquist diagram and two inflection points on the Bode plots similar to samples AM1 and AM2. After 6 h of immersion, the second semicircular loop on the Nyquist diagram has a significant expansion compared to the first half semicircular loop. It shows that the corrosion products formed on the surface of the AM3 sample after 6 h of immersion contribute to a significant reduction in the corrosion rate of Al-Mg coating compared to the AM1 and the AM2 samples.

The measured corrosion current density of sample AM3 after 6 h of immersion was 2.7 μA/cm^2. Meanwhile, the corrosion current density after 6 h of immersion in the NaCl solution of samples AM1 and AM2 were 3.3 μA/cm^2 and 27.1 μA/cm^2, respectively. Corrosion products on the coating surface increased over time, causing the phase angle at high frequencies to increase with time (Fig. 8c). The solution/coating dual layer capacitance ($Q1$) increased sharply from 0.016×10^{-3} to 51.95×10^{-3} Fcm^{-2} s^{-n} over the immersion period from 6 to 24 h. That shows the exposure time of the alloy coating in the 3.5 wt.% NaCl solution was much because the corrosion products formed on the surface were not a lot. Meanwhile, the decrease in the double layer capacitance of the solution/inner surface ($Q2$) indicates that the coating corrosion products have contributed to limiting the penetration of NaCl solution into the coating. During the sample immersion period from
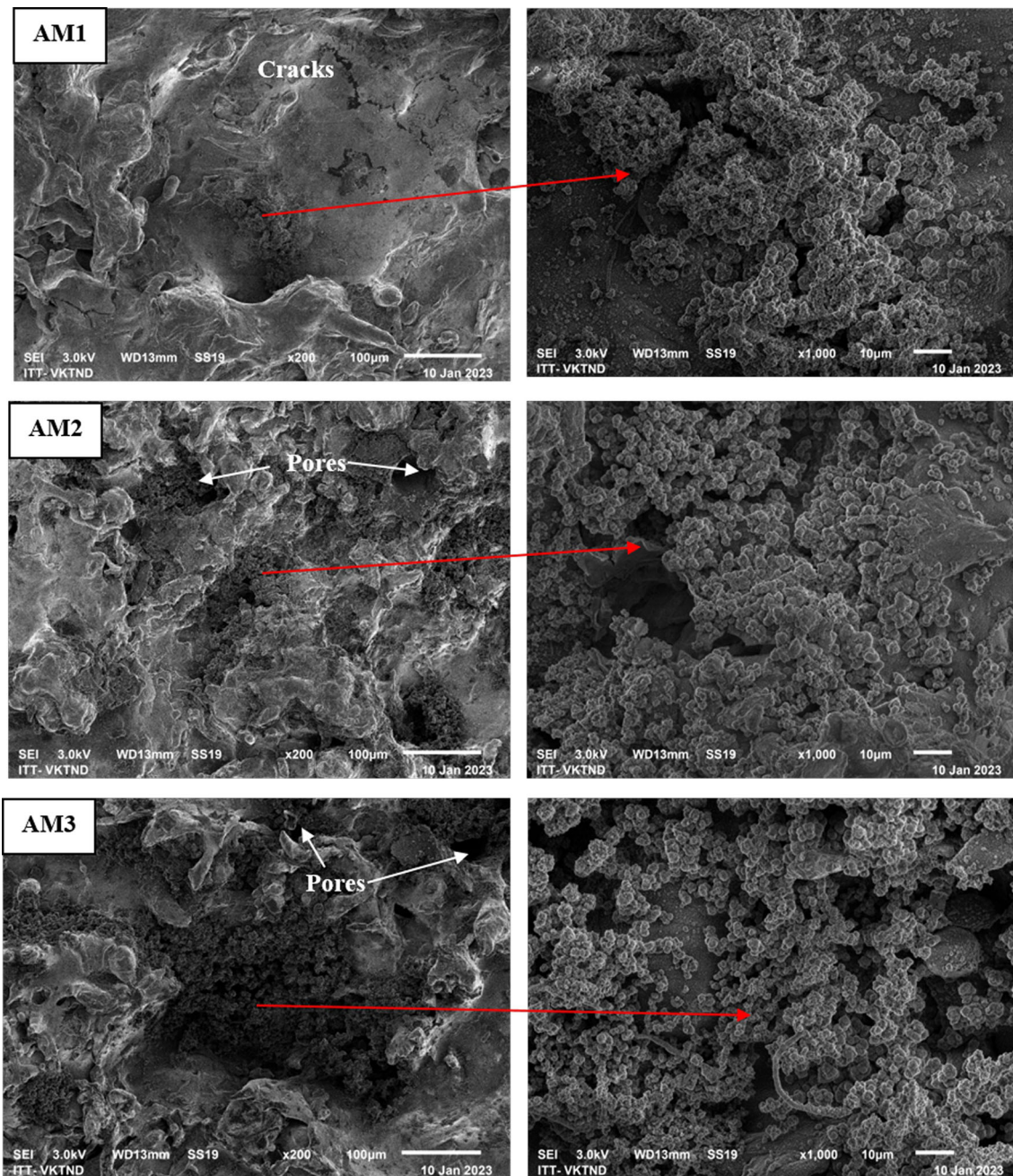
Fig. 10 Surface morphology of Al-Mg alloy coatings after corrosion test

24 to 48 h, the $Q1$ of the AM3 sample decreased sharply. It shows that the more and more corrosion products formed on the surface have significantly limited the exposure time of Al-Mg alloy coating in the 3.5 wt.% NaCl solution, causing the corrosion density of the AM3 sample to decrease from 3.9 to 2.1 $\mu A/cm^2$. In addition, the Bode diagram of Fig. 7(c) shows that the phase angle of the first layer of AM3 sample moved to higher angles, and at the same time, the total pore impedance increased sharply from 1089 to 8936 Ω cm^2 during the sample immersion time

from 24 to 48 h, showing that the corrosion product deposited in the pores, which reduced the corrosion density of the coating from 3.9 to 2.1 $\mu A/cm^2$. After the sample immersion period of 48, 96, and 240 h the half-semicircular loop on the Nyquist diagram and the current density tend to decrease, it may be a part of the corrosion product of the Al-Mg alloy coating being degraded and detach from the surface due to poor adhesion of the corrosion product to the surface.
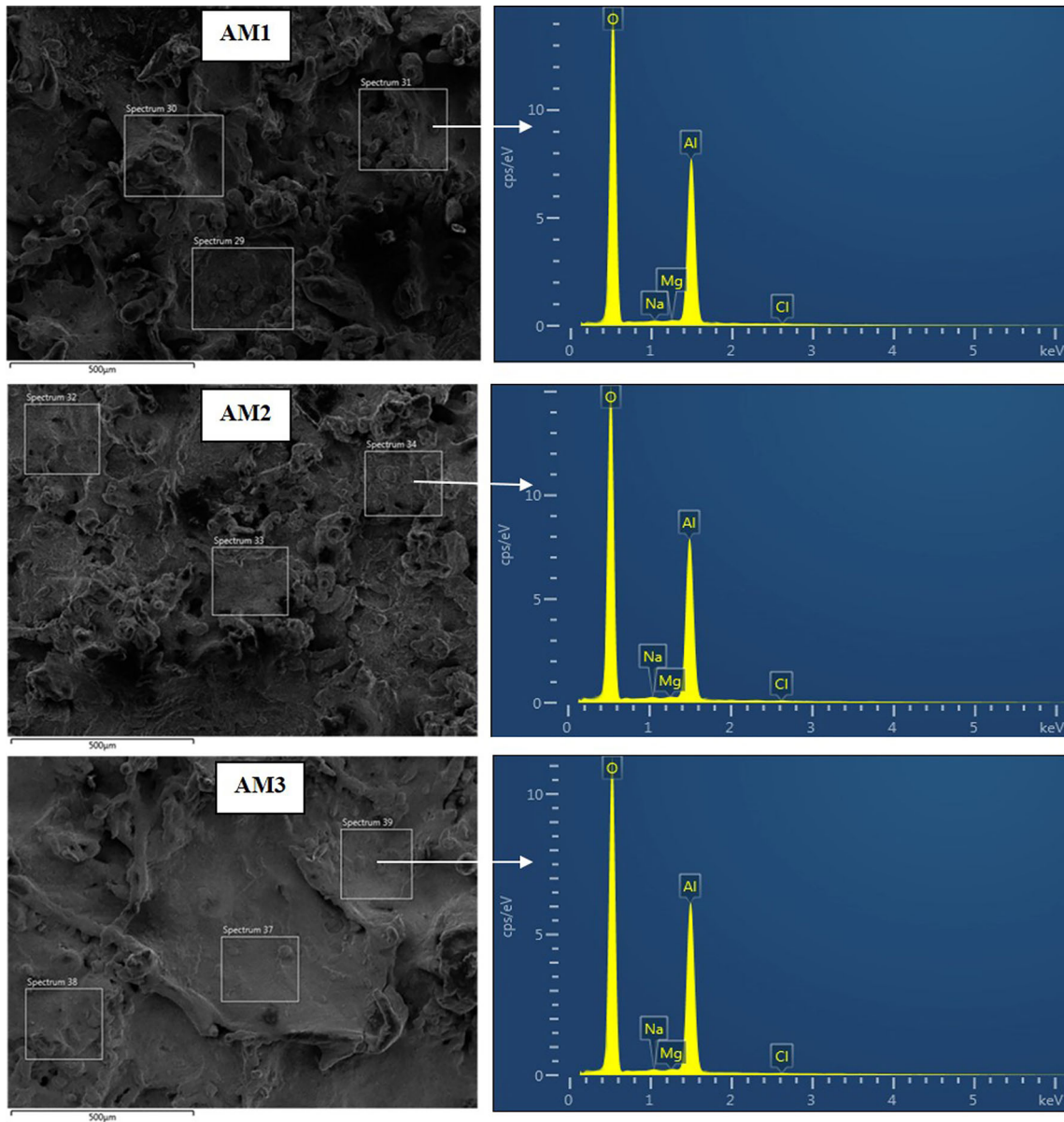
Fig. 11 SEM-EDS analysis to determine chemical elemental composition on the surface of coatings after the corrosion test

Table 5 Chemical compositions on the surface of samples after the exposure time

No.	Element	Weight, %		
		AM1	AM2	AM3
1	Al	45.98	44.54	43.9
2	Mg	1.36	1.17	1.71
3	O	52.17	53.54	53.77
4	Na	0.11	0.29	0.28
5	Cl	0.38	0.46	0.34
6	Tổng	100	100	100

Coatings Characterization after the Corrosion Test

Surface Morphology and Chemical Composition of the Coating after the Corrosion Test

After 240 h of corrosion test in NaCl solution, the surface of the samples had a significant change from the original surface. The surface of sample AM1 appeared to have relatively obvious cracks and spherical corrosion products, about 1 μm in size, which were deposited in some areas on the coating surface. In addition, there were not many corrosion products on the surface of the AM1 sample, so the
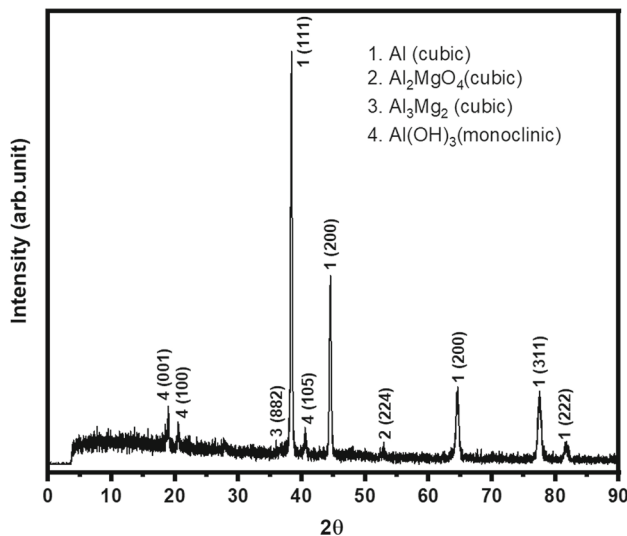
Fig. 12 XRD pattern of corrosion products formed on the coating surface (AM3) after the corrosion test

sample's corrosion rate did not change much after 24 h of immersion (Table 3). Meanwhile, after the corrosion test, the AM2 sample surface has no surface cracks. However, on the surface of the AM2 sample, there are many pores and many corrosion products agglomerated on the surface. This demonstrates that sample AM2 has corrosive qualities that change over time since the corrosion properties of the coating in NaCl solution have altered over time due to the corrosion products on the surface. On the other hand, the surface of the AM2 sample contains many corrosion products, especially at the position of the pores of the coating. It shows that the corrosion rate of sample AM2 is higher than that of sample AM1 due to the higher porosity of the coating (Table 3). For sample AM3, the results showed that the coating surface did not have cracks.

On the surface, many corrosion products have accumulated in clusters, changing the surface properties of the coating, especially the corrosion properties. The results of the study in Table 3 show that the Al-Mg coating corrosion rate changed over time. It proves that the corrosion products formed on the surface have a considerable influence on the Al-Mg alloy coating corrosive properties. On the surface of the AM3 sample, there are fewer pores than that of AM1 and AM2 (Fig. 10), so the corrosion rate of the AM3 sample is significantly smaller than that of those two samples (Table 3). Figure 11 shows the result of SEM-EDS analysis to determine the composition of chemical elements present on the surface of the Al-Mg alloy coating after 240 h of immersion in 3.5 wt.% NaCl solution. The immersed samples were measured in three different areas of the surface, then the measurement results were averaged. Analytical results (Table 5) showed that the Al and Mg elemental fractions after the corrosion test on the surface of

the samples were much reduced compared to that before the test. Meanwhile, the O element on the surface of the samples after the corrosion test was much larger than before the test. The lower Al and Mg elements content on the surface of the sample after 240 h of immersion in NaCl solution coming from the corrosion or obscured by corrosion products. Corrosion products formed on the surface are oxygen compounds, so the O elemental composition on the surface of Al-Mg alloy coating has increased after 240 hof exposure. Corrosion products of Al-Mg alloy coating in the solution of 3.5 wt.% NaCl after 240 h of immersion were studied by x-ray diffraction (XRD).

The Phase Compositions on the Coating Surface after the Corrosion Test

The results of phase composition analysis on the coating surface were determined by x-ray diffraction (XRD). Figure 12 illustrates the corrosion products' XRD pattern form on the coating. Analytical results show that, after the corrosion test, and apart from phase components Al (cubic), Al_2MgO_4 (cubic), and Al_3Mg_2 (cubic) similar to the phase components exist on the surface coating of the samples Al-Mg alloy before the corrosion test, $Al(OH)_3$ phase component was found in the corrosion products. As detected previously, the corrosion products of Al-Mg alloy coating immersed in NaCl Al-Mg solution include compounds such as $Mg(OH)_2$, $Al(OH)_3$, $Al(OH)_2Cl$, $Al(OH)Cl_2$ (Ref 50). However, on the x-ray diffraction pattern, the peaks of the crystals of $Al(OH)_2Cl$, $Al(OH)Cl_2$, and $Mg(OH)_2$ were not found, possibly due to low concentrations below the detection threshold or the remaining corrosion products being amorphous.

Conclusions

The Al-Mg alloy coatings were deposited from Al-Mg alloy wire containing 5 wt.% Mg with a diameter of 2 mm by using a twin-wire electric arc spray process with different spray parameters. The results show that spray current, pneumatic pressure, and standoff distance affect the structure and corrosion resistance of the coating in 3.5 wt.% NaCl solution.

- The sprayed coating at a spray current of 300 A, pneumatic pressure of 5.5 bar, and stand-off distance of 160 mm has a more homogeneous surface structure and better corrosion protection than the remaining coatings. Moreover, the lowest porosity (7.38%) of the coating and Al (85.78 wt.%) and Mg (3.47 wt.%) maximum elemental contents in the coating were also obtained at these spraying parameters.

- The corrosion resistance of coating samples changes over time due to the influence of corrosive products that have agglomerated on the coating surface. After 240 h of immersion in 3.5 wt.% NaCl solution, microcracks appeared on the surface of the fabricated coating at 150A spray current, 4.0 bar spray pressure, and 100 mm spray distance. Meanwhile, no cracks were observed on the surface of other coating samples. In addition, XRD analysis results showed that the corrosion product on the surface of the coatings is mainly $Al(OH)_3$.

References

1. S.A. Galedari, A. Mahdavi, F. Azarmi, Y. Huang, and A. McDonald, A Comprehensive Review of Corrosion Resistance of Thermally Sprayed and Thermally-Diffused Protective Coatings on Steel Structure, *J. Therm Spray Tech.*, 2019, **28**, p 645-677.

2. M.R. Dhanak and N.I. Xiros, *Springer Handbook of Ocean Engineering*, Springer, 2016.

3. F. Deng, Y. Huang, F. Azarmi, and Y. Wang, Pitted Corrosion Detection of Thermal Sprayed Metallic Coatings Using Fiber Bragg Grating Sensors, *Coatings*, 2017, **7**(3), p 35.

4. P.A. Sørensen, S. Kiil, K. Dam-Johansen, and C.E. Weinell, Anticorrosive Coatings: A Review, *J. Coat. Technol. Res.*, 2009, **6**(2), p 135-176.

5. Y.T. Li and B.R. Hou, Anticorrosion Mechanism of Thermal Spraying Coatings of Zinc and Aluminum and of Alloys Made of the Same in Marine Environment: A Review, *Mater. Prot. Wuhan*, 2005, **38**(9), p 30.

6. A. Farooq, M. Hamza, Q. Ahmed, and K.M. Deen, Evaluating the Performance of Zinc and Aluminum Sacrificial Anodes in Artificial Seawater, *Electrochim. Acta*, 2019, **314**, p 135-141.

7. E. Dalledone, M. Barbosa, and S. Wolynec, Zinc-55% Aluminum 16% Silicon Coating Compared with Zinc Coating, *Mater. Perform.*, 1995, **34**(7), p 1203.

8. A. Marder, The Metallurgy of Zinc-Coated Steel, *Prog. Mater. Sci.i.*, 2000, **45**(3), p 191-271.

9. Z. Panossian, L. Mariaca, M. Morcillo, S. Flores, J. Rocha, J. Pena, F. Herrera, F. Corvo, M. Sanchez, and O. Rincon, Steel Cathodic Protection Afforded by Zinc, Aluminium and Zinc/Aluminium Alloy Coatings in the Atmosphere, *Surf. Coat. Technol.*, 2005, **190**(2-3), p 244-248.

10. A. Gulec, O. Cevher, A. Turk, F. Ustel, and F. Yilmaz, Accelerated Corrosion Behaviors of Zn, Al and Zn/15Al Coatings on a Steel Surface, *Mater. Tehnol.*, 2011, **45**(5), p 477-482.

11. Y. Li, Corrosion Behaviour of Hot Dip Zinc and Zinc-Aluminium Coatings on Steel in Seawater, *Bull. Mater. Sci.*, 2001, **24**(4), p 355-360.

12. G. Kong and R. White, Toward Cleaner Production of Hot Dip Galvanizing Industry in China, *J. Clean. Prod.*, 2010, **18**(10-11), p 1092-1099.

13. S. Egtvedt, Thermally Sprayed Aluminum (TSA) with Cathodic Protection as Corrosion Protection for Steel in Natural Seawater: Characterization of Properties on TSA and Calcareous Deposit, Institutt for materialteknologi, 2011.

14. E.A. Esfahani, H. Salimijazi, M.A. Golozar, J. Mostaghimi, and L. Pershin, Study of Corrosion Behavior of Arc Sprayed Aluminum Coating on Mild Steel, *J. Therm. Spray Technol.*, 2012, **21**(6), p 1195-1202.

15. W. Gu, D. Shen, Y. Wang, G. Chen, W. Feng, G. Zhang, S. Fan, C. Liu, and S. Yang, Deposition of Duplex Al_2O_3/Aluminum Coatings on Steel Using a Combined Technique of Arc Spraying and Plasma Electrolytic Oxidation, *Appl. Surf. Sci.*, 2006, **252**(8), p 2927-2932.

16. E. Irissou, J.G. Legoux, B. Arsenault, and C. Moreau, Investigation of $Al-Al_2O_3$ Cold Spray Coating Formation and Properties, *J. Therm. Spray Technol.*, 2007, **16**(5-6), p 661-668.

17. H.B. Choe, H.S. Lee, and J.H. Shin, Experimental Study on the Electrochemical Anti-Corrosion Properties of Steel Structures Applying the Arc Thermal Metal Spraying Method, *Materials*, 2014, **7**(12), p 7722-7736.

18. H. Yang, Z. Yao, D. Wei, W. Zhou, G. Yin, and L. Feng, Anti-corrosion of Thermal Sprayed Al-Zn-Si Coating in Simulated Marine Environments, *Surf. Eng.*, 2014, **30**(11), p 801-805.

19. R.M.P. Rodriguez, R.S. Paredes, S.H. Wido, and A. Calixto, Comparison of Aluminum Coatings Deposited by Flame Spray and by Electric Arc Spray, *Surf. Coat. Technol.*, 2007, **202**(1), p 172-179.

20. E. Irissou and B. Arsenault, *Corrosion Study of Cold Sprayed Aluminum Coatings onto Al-Lithium (Al 2195) and Al 7075 Alloy Substrates*, NRC Publications Archive, Ottawa, 2007.

21. H.M. Su, W.Y. Bin, K.S. Cheol, Y.J. Jeong, J.S. Ki, and K.S. Jong, Effects of Thickness of Al Thermal Spray Coating for STS 304, *T. Nonferr. Metal. Soc.*, 2009, **19**(4), p 925-929.

22. I. Park and S. Kim, Cavitation Damage Behavior in Seawater for Al-Mg Alloy Arc Thermal Spray Coating with Mg Content, *Acta Phys. Pol. A*, 2016, **129**(4), p 572-577.

23. Y. Takeyoshi, S. Takase, Y. Shimizu, M. Sueyoshi, and Y. Uchida, Corrosion Protection of Steel by Al-Mg Plasma Spray Coating, Meeting Abstracts, *The Electrochemical Society.* 2010, p910-910.

24. D. Mari, L. Miguel, and C.E. Nebel, *Comprehensive Hard Materials*, Newnes, New York, 2014.

25. M.H. AbdMalek, N.H. Saad, S.K. Abas, and N.M. Shah, Thermal arc spray overview, in IOP Conference Series: Materials Science and Engineering, Publishing, IOP 2013, p012028.

26. R. Bolot, R. Bonnet, G. Jandin, and C. Coddet, Application of CAD to CFD for the Wire Arc Spray Process, *J. Therm. Spray Technol.*, 2001, **2**, p 889-894.

27. S. Kuroda, J. Kawakita, and M. Takemoto, An 18-year Exposure Test of Thermal-Sprayed Zn, Al, and Zn-Al Coatings in Marine Environment, *Corrosion*, 2006, **62**(7), p 635-647.

28. A.G. Cevher, A. Turk, F. Ustel, and F. Yılmaz, Accelerated Corrosion Behaviors of Zn, Al and Zn/15Al Coatings on a Steel Surface, *Science*, 2011, **2**, p 1-1008.

29. L. Qiao, Y. Wu, J. Duan, W. Gao, and S. Hong, Corrosion Behavior of Arc-Sprayed Pore Sealed Zn and Al Coatings in

Seawater Containing Sulfate-Reducing Bacteria (SRB), *J. Therm. Spray Technol.*, 2021, **30**(6), p 1557-1565.

30. S. Hong, Y. Wu, W. Gao, J. Zhang, and Y. Qin, Corrosion Behavior of Arc-Sprayed Zn-Al Coating in the Presence of Sulfate Reducing Bacteria in Seawater, *J. Mater. Eng. Perform.*, 2015, **24**(11), p 4449-4455.

31. H. Katayama and S. Kuroda, Long-Term Atmospheric Corrosion Properties of Thermally Sprayed Zn, Al and Zn-Al Coatings Exposed in a Coastal Area, *Corros. Sci.*, 2013, **76**, p 35-41.

32. H.S. Lee, J.K. Singh, M.A. Ismail, C. Bhattacharya, A.H. Seikh, N. Alharthi, and R.R. Hussain, Corrosion Mechanism and Kinetics of Al-Zn Coating Deposited by arc Thermal Spraying Process in Saline Solution at Prolong Exposure Periods, *Sci. Rep.*, 2019, **9**(1), p 1-17.

33. H. Hu, P. Zhang, D. Wei, and F. Su, Microstructure and Corrosion Behavior of Arc Sprayed Zn-xAl (x= 15, 30, 50) Alloy Coatings in NaCl Solution, *Mater. Res. Express*, 2019, **6**(10), p 1065-1067.

34. R.D. Yasoda, Y. Huang, and X. Qi, Corrosion Performance of Wire Arc Deposited Zinc Aluminum Pseudo Alloy and Zinc 15 Aluminum Alloy Coatings on Steel in Chloride Environment, *J Therm Spray Tech.*, 2022, **31**, p 1918-1933.

35. I. Park and S. Kim, Cavitation Damage Behavior in Seawater for Al-Mg Alloy Arc Thermal Spray Coating with Mg Content, *Acta Phys. Pol. A.*, 2016, **129**(4), p 572-577.

36. ISO 1463:2003, Metallic and oxide coatings: Measurement of coating thickness—Microscopical method.

37. ASTM E2109-01, Test Methods for Determining Area Percentage Porosity in Thermal Sprayed Coatings.

38. ASTM G59-97, Standard Test Method for Conducting Potentiodynamic Polarization Resistance Measurements.

39. A.L. Ortegaa, R. Bayón, and J.L. Aranab, Evaluation of Protective Coatings for Offshore Applications: Corrosion and Tribocorrosion Behavior in Synthetic Seawater, *Surf. Coat. Technol.*, 2018, **349**, p 1083-1097.

40. J.R. Davis, *Handbook of Thermal Spray Technology*, ASM International, New York, 2004.

41. B. Jahani, A. Brooks, and F. Azarmi, Development of Antibacterial Surfaces Via Thermal Spray Coating Techniques, *Biomed. SciInstrum.*, 2018, **54**(1), p 116-122.

42. R. Ahmed, O. Ali, C.C. Berndt, and A. Fardan, Sliding Wear of Conventional and Suspension Sprayed Nanocomposite WC-Co Coatings: An Invited Review, *Therm. Spray Tech.*, 2021, **30**, p 800-861.

43. A.C. Savarimuthu, H.F. Taber, I. Megat, J.R. Shadley, E.F. Rybicki, W.C. Cornell, W.A. Emery, D.A. Somerville, and J.D. Nuse, Sliding Wear Behavior of Tungsten Carbide Thermal Spray Coatings for Replacement of Chromium Electroplate in Aircraft Applications, *Therm. Spray Tech.*, 2001, **10**, p 502-510.

44. G. Bolelli, V. Cannillo, L. Lusvarghi, and S. Ricco, Mechanical and Tribological Properties of Electrolytic Hard Chrome and HVOF-Sprayed Coatings, *Surf. Coat. Technol.*, 2006, **200**, p 2995-3009.

45. E. Romhanji and M. Popović, Problems and Prospect of Al-Mg Alloys Application in Marine Constructions, *MJoM*, 2006, **12**(4), p 297-307.

46. A. Duran, R. Dif, New Alloy Development at Pechiney, a New Generation of 5383 in Conf. Proc. FAST 2001, Southampton, Southampton University, Ed. by P.A. Wilson, G.E. Hearn, Sept. 2001.

47. A. Haszler, Latest Aluminium Alloy Developments for Plate Applications in High Speed Ferry and Aircraft Structures, Conf. Proc. Aluminum 97, Aluminum Technology and Markets for the New Century, 24-25 Sept. 1997, Messe Essen, Germany, p 2-9.

48. R.G. Echaniz, P. Refait, M. Jeannin, R. Sabot, S. Paul, and R. Thornton, Study of Cathodic Reactions in Defects of Thermal Spray Aluminium Coatings on Steel in Artificial Seawater, *Corros. Sci.*, 2021, **187**, p 109514.

49. M.E. Orazem, B. Tribollet, Electrochemical Impedance Spectroscopy, 2008.

50. BT-Lab & EC-Lab, Data Analysis and Processes, Version 11.00 ,2015.

51. B. Wang, L. Zhang, Y. Su, Y. Xiao, and J. Liu, Corrosion Behavior of 5A05 Aluminum Alloy in NaCl Solution, *Acta Metall. Sin.*, 2013, **26**(5), p 581-587.

52. Q. Jiang, Q. Miao, F. Tong, Y. Xu, B.L. Ren, Z.M. Liu, and Z.J. Yao, Electrochemical Corrosion Behaviour of Arc Sprayed Al-Zn-Si-RE Coatings on Mild Steel in 3.5% NaCl Solution, *Trans. Nonferrous Metals Soc. China*, 2014, **24**, p 2713-2722.

53. W. Liu, Q. Zhou, L. Li, Z. Wu, F. Cao, and Z. Gao, Effect of Alloy Element on Corrosion Behavior of the Huge Crude Oil Storage Tank Steel in Seawater, *J. Alloys Compd.*, 2014, **598**, p 198-204.

54. N. Imaz, M. Ostra, M. Vidal, J.A. Díez, M. Sarret, and E.G. Lecina, Corrosion Behaviour of Chromium Coatings Obtained by Direct and Reverse Pulse Plating Electrodeposition in NaCl Aqueous Solution, *Corros. Sci.*, 2014, **78**, p 251-259.

55. F. El-TaibHeakal, N.S. Tantawy, and O.S. Shehta, Influence of Chloride Ion Concentration on the Corrosion Behaviour of Al-Bearing TRIP Steels, *Mater. Chem. Phys.*, 2011, **130**, p 743-749.

56. D. Yang, O. Rosas, and H. Castaneda, $FeCO_3$ Layer Evolution for API 5L X52 Steel in Carbon Dioxide Saturated NaCl Brine in the Presence of 1-Decyl-3-Methylimidazo-Lium Chloride, *Corros. Sci.*, 2014, **87**, p 40-50.

57. E.A. Esfahani, H. Salimijazi, M.A. Golozar, J. Mostaghimi, and L. Pershin, Study of Corrosion Behaviour of Arc Sprayed Aluminium Coating on Mild Steel, *J. Therm. Spray Technol.*, 2012, **21**, p 1195-1202.